NASA Technical Memorandum 105952
AIAA–93–0029

Close-up Analysis of Aircraft Ice Accretion

R. John Hansman, Kenneth S. Breuer,
and Didier Hazan
Massachusetts Institute of Technology
Cambridge, Massachusetts

and

Andrew Reehorst and Mario Vargas
Lewis Research Center
Cleveland, Ohio

Prepared for the
31st Aerospace Sciences Meeting and Exhibit
sponsored by the American Institute of Aeronautics and Astronautics
Reno, Nevada, January 11–14, 1993

NASA

CLOSE-UP ANALYSIS OF AIRCRAFT ICE ACCRETION

R. John Hansman, Jr., Kenneth S. Breuer, and Didier Hazan
Department of Aeronautics and Astronautics
Massachusetts Institute of Technology
Cambridge, Massachusetts 02139

and

Andrew Reehorst and Mario Vargas
National Aeronautics and Space Administration
Lewis Research Center
Cleveland, Ohio 44135

Abstract

Various types of ice formation have been studied by analysis of high magnification video observations. All testing was conducted in the NASA Lewis Research Center's Icing Research Tunnel (IRT). A faired 8.9 cm (3.5 in.) diameter metal-clad cylinder and a 5.1 cm (2 in.) aluminum cylinder were observed by close-up and overview video cameras for several wind tunnel conditions. These included close-up grazing angle, close-up side view, as well as overhead and side overview cameras. Still photographs were taken at the end of each spray along with tracings of the subsequent ice shape. While in earlier tests only the stagnation region was observed, the entire area from the stagnation line to the horn region of glaze ice shapes was observed in this test. Two modes of horn formation have been identified within the range of conditions observed. In the horn region, Horn Type A ice is formed by "dry" feather growth into the flow direction and Horn Type B is formed by a "wet" growth normal to the surface. The feather growth occurs when the freezing fraction is near unity and roughness elements exist to provide an initial growth site.

Introduction

Accurate modeling of "horn" growth under glaze icing conditions has been a consistent problem for analytical ice accretion modeling efforts.[1,2] Once the horns have started, the growth is fairly well understood; however, the physical mechanisms which cause horn initiation are not clear. In order to study horn initiation, high magnification video observations of the ice surface were made at the horn initiation sites on simple cylindrical bodies. These observations were supported by simultaneous overview video observations.

Background

Previously reported efforts have investigated the ice accretion process via close-up photographic methods near the stagnation region of the test body.[1,2] These studies have described the movement of water on the surface, the growth of ice, and the development of roughness on the ice surface. Due to testing constraints, these earlier observations were limited to the stagnation region. Through the use of multiple high magnification video cameras viewing the body from multiple angles, the work presented here attempts to extend these prior studies to include the off-stagnation regions where glaze horns originate. The analysis of these data is used to determine several overall ice shape accretion mechanisms that complement the roughness formation mechanisms determined from earlier work.[1,2]

Test Apparatus

In June and July 1992 a close-up video test was conducted in the NASA Lewis Research Center's Icing Research Tunnel (IRT) to expand on prior stagnation region tests. The IRT is the world's largest refrigerated icing tunnel, capable of producing artificial icing clouds of varying severity over a range of temperatures and airspeeds[3] (Fig. 1). The models used for this test were a 5.1 cm (2 in.) diameter aluminum cylinder and a 8.9 cm (3.5 in.) diameter aluminum-skinned faired cylinder. To examine a range of ice formations, a test matrix was developed that covered various airspeeds, temperatures, cloud liquid water content and droplet size. During each icing spray the model was observed with two close-up video cameras (stagnation and horn regions) and an overview video camera. After each spray, the model was photographed with a 35-mm handheld camera and tracings were made of the resultant ice shape.

Video Camera Setup

The video imaging techniques used during this test have evolved from the film techniques originally used by Olsen and Walker.[1] Among the test rigs used previously was an assembly consisting of a wooden 8.9 cm (3.5 in.) diameter faired cylinder model and a movie camera and a strobe light mounted to the model. In 1991 this rig was modified to allow the use of video as the recording media. This system used the original wooden 8.9 cm (3.5 in.) faired cylinder model and strobe and replaced the movie camera with a CCD video camera and an SVHS video cassette recorder. Use of video instead of film allowed real-time monitoring of the recording image and allowed much easier data analysis. To ensure ice accretion at stable conditions, a shield was added to the system. The shield was retracted after the IRT icing cloud had stabilized at the desired condition. Results and analysis from this testing were reported by Hansman.[2]

The rig used in 1991 had the camera assembly and strobe so close to the model that it was felt that the flowfield was affected and this influenced the ice shapes. In order to reduce interference, the camera assembly and lighting system were separated from the model (Fig. 2). Replacing the strobe lighting system, a 575 W Hydrargyrum medium-arc-length iodide (HMI) lamp was mounted above the IRT test section ceiling to illuminate the model. The close-up camera was moved into a fairing mounted to the tunnel floor on a turntable. Figure 3 shows the camera without the fairing and Fig. 4 shows the camera and fairing assembly. It was planned to use the fairing camera to view off the model stagnation line by rotating the turntable. However, the camera fairing vibrated at angle of attack preventing adequate imaging of the off-stagnation region. To enable viewing away from the stagnation line, a telescopic close-up camera was located in the tunnel control room window (Fig. 5). The telescopic close-up lens was assembled by adding a sufficient number of extension tubes to a telephoto lens to produce the desired level of magnification. Magnification levels of approximately 0.7 were used (Magnification level = image length in the camera/field of view length at the model). Again, a retracting shield was used to ensure a stabilized cloud was used to accrete the ice. The model was hung from the tunnel ceiling and stabilized to the floor to eliminate vibration. The models used were the 8.9 cm (3.5 in.) model now clad in aluminum and a 5.1 cm (2 in.) diameter aluminum cylinder.

Ice Shape Documentation

Photographs and ice-shape tracings were made at the end of each spray to document the final ice shape. At the end of a spray, the tunnel fan was brought to idle power to allow personnel entry into the test section. The ice accretion was first documented by 35-mm photos and then a cut was made through the ice accretion with a heated aluminum template. A cardboard template was then placed in the cut and aligned to allow a pencil tracing of the ice shape onto the template (Fig. 6).

Testing Matrix

The test matrix was developed to produce as wide a variety of ice types as possible within the time constraints of the testing period.

June and July 1992 close-up video test matrix	
Parameter	Range
Velocity, m/s (mph)	44 (100), 67 (150), 89 (200)
Temperature, °C (°F)	-26 (-15), -20 (-5), -15 (-5), -9 (15), -4 (25)
Liquid water content, g/m^3	0.32, 0.5, 0.7, 0.75, 1.0
Mean volume diameter, μm	15, 20

Observations

Ice Accretion Types Observed

Four generic types of ice accretion were observed. Ice shape tracings from examples of each type are shown in Fig. 7 for the 8.9 cm (3.5 in.) cylinder. At cold temperatures, *Rime* accretions were observed with the characteristic white ice and conformed ice shape. At warmer temperatures *Mixed* ice was observed along with two types of *Glaze Horn* growth. *Mixed* ice accretions are characterized by clear glaze ice in the stagnation region and opaque rime like ice in the off stagnation regions. The Horn accretion type labeled as *Horn A* growth is characterized by horns which are fairly close to the stagnation region and tend to grow into the flow. *Horn B* growth is characterized by widely spread horns which initiate further back and tend to grow more radially. *Horn B* growth occurs only under very high liquid water conditions at warm temperatures.

Observations of Feather Growth in the Horn Region

The most significant observation of the high-magnification system was the prevalence of "feather" growth in the horn regions. In all *Mixed*, *Horn A* and *Rime* cases, "feather" growth was observed in the horn regions. Several examples of "feathers" are shown in Figs. 8 and 9 taken with the high magnification video in the horn region. (Note that the flow is from the left in the figures.) Feather growth had been previously observed for low velocity rime accretions and is often observed downstream of the primary accretion in rime ice cases. However, feather growth had not been directly reported before for horn growth.

The mechanism for feather growth has been modeled by Personne[4] as a simple rime growth where each droplet sticks upon impact. The feather spreads laterally as it grows into the flow resulting in a characteristic feather shape. The postulation of feather growth is supported by the excellent correlation between the shape predicted by the Personne ballistic accretion model and the contour tracings of a typical feather observed growing in the horn region shown in Fig. 10.

The observed feathers typically appeared to be rime ice. Since rime growth implies complete freezing of the impinging water, the growth rate of the feather should be proportional to the mass flux $\dot{M}$ which is the product of the liquid water content LWC and the velocity V.

$$\dot{M} = \mathrm{LWC(V)}$$

This can be seen in Fig. 11 which plots examples of feather size as a function of time for cases with different velocities but similar mass fluxes (i.e., LWC = 1.0 gm/m^3 at 44 m/s (100 mph) and LWC = 0.5 gm/m^3 at 89 m/s (200 mph)). While the initial growth rates vary the steady state growth rates are quite similar. The relationship between feather growth rate and mass flux is displayed in Fig. 12 which plots the feather growth rates measured for the different mass fluxes observed. It should be reiterated that feather growth is not limited to rime ice accretions as had been previously thought. Feathers were also observed to grow out of clear glaze ice. An example is shown in Fig. 13 where a feather is observed to grow out of a clear glaze substrate.

Feather Growth Initiation

The initiation of feather growth can be seen in Figs. 14 and 15. By reviewing the video observations in reverse, each feather can be traced to an original nucleation site. If the initial surface has irregularities, such as those seen in Fig. 14, these will be the nucleation sites. If the initial surface is smooth, the natural ice surface roughness will grow until the local roughness elements are sufficient to provide nucleation sites for feather growth. Note that the difference in nucleation site density in Figs. 14 and 15 results in different feather densities.

Feathers appear to start to grow when the nucleation sites penetrate into the turbulent boundary layer. The top of the nucleation roughness elements will see higher local velocity than the lower surrounding surface. This higher velocity results in a higher convective heat transfer coefficient, h, and higher local collection efficiency, β, at the top of the roughness element. The higher heat transfer will result in a higher freezing fraction. Once the freezing fraction approaches unity, the feather growth will begin in the direction of the local flow.

Feather growth will continue as long as droplets are impinging. However, since the feathers tend to spread out laterally, when the feather density is high, adjacent feathers will tend to merge.

Effect of Ice Type on Horn Region Ice Growth

Rime Accretions

For *Rime* accretions, feathers were observed in the off-stagnation regions although no horns were observed. The feather growth shown in Fig. 15 was a *Rime* case. A characteristic of feather growth in *Rime* accretions was that the feathers were brittle and often closely spaced. The feathers were frequently observed in the video to break if they grew too large or too far above the surface. As the feathers merge, voids are left near the roots of adjacent feathers causing the bulk density of the feather accretion to be lower than glaze ice.

Mixed Accretions

Mixed ice accretions are characterized by clear growth in the stagnation region and an opaque *Rime* growth in the off-stagnation zones. Feathers were observed in these opaque regions by the close-up video. The clear ice is thought to be due to a low freezing fraction in the stagnation region which results in wet growth with the unfrozen water running back to downstream regions. This reduced freezing fraction in the stagnation region can be seen as a product of reduced heat transfer due to the laminar boundary layer, elevated water load, and higher local temperatures. This growth is normal to

the surface and the growth rate is controlled by the local heat transfer behavior of the surface.

At some point in the evolution of *Mixed* ice accretions, the roughness elements which are generated aft of the boundary layer transition[2] become large enough to act as nucleation sites for feather growth. The feathers grow rapidly into the direction of local airflow as in the *Rime* case. However, the density of nucleation sites is often lower. The interstitial gaps between adjacent feathers are observed to fill with unfrozen water running back from the stagnation region. Since the runback water freezes slowly resulting in clear ice the resulting accretion will have streaks of clear and opaque ice as observed by Olsen.[1]

For reasons as yet unknown, in *Mixed* ice the feather growth slows as the feathers reach the upstream boundary of the accretion. Feathers initiating further aft continue to grow resulting in the fairly flat leading edge observed in these accretions (Fig. 7). The mechanisms which control this process are not well understood at this point but are thought to be due to the interaction between feathers and runback growth.

Horn *Type A* Accretions

Horn *Type A* growth is quite similar to the *Mixed* growth process; however, the feather growth does not slow but continues to grow into the flow resulting in the characteristic *Type A* horn shape seen in Fig. 7. As noted above, the mechanism which differentiates *Type A* and *Mixed* growth is not clear. However, *Type A* growth is normally observed for higher liquid water contents or larger droplet sizes under otherwise similar conditions. This indicates that the relative growth rates between the stagnation region (which is controlled by heat transfer), and the feathers (which are controlled by mass flux) may be important factors or the *Type A* accretions may simply be a later evolution of the *Mixed* ice.

Horn *Type B* Accretions

Horn *Type B* growth is only observed at very warm temperatures and high liquid water contents. In this type of accretion, no feather growth was observed. The surface was observed by close-up video to be very wet, indicating that the heat transfer is insufficient to raise the freezing fraction to unity within the impingement region.

In overview video observations, the runback region was seen to initially spread behind the impingement region. The *Type B* horns were observed to initiate at the downstream boundary of the runback region which was often quite irregular due to the runback pattern. This runback pattern has been examined by Al-Khalil.[5] The extent of the runback region was observed to increase with liquid water content, consequently, the horns were observed to spread as the liquid water content is increased. This can be seen in Fig. 16.

Implications for Ice Accretion Modeling

The observations of prevalent feather growth in the horn regions may explain some of the difficulty ice accretion codes have had for glaze ice conditions. Current codes either accrete the ice in a direction normal to the surface[6] or into the direction of flow.[7] However, the observations discussed above indicate both surface-normal and into-flow growth occur in different regions. For accretion codes such as LEWICE, where the computational grid structure is normally large compared with the roughness element size, the different growth regions can be included in a manner such as that shown in Fig. 17. If the freezing fraction in the stagnation region is less than unity then there will be a wet glaze region where the growth will be normal to the surface. In the downstream regions, if feather growth occurs (i.e., *Rime*, *Mixed*, or *Type A* Horns), the growth will be into the flow. Some care with the computational geometry is required as the surface-normal and into-flow growth regions will tend to converge. If feather growth does not occur, then *Type B* Horns would be predicted.

The criterion for feather growth is that the freezing fraction at the top of a typical roughness element is unity. If the element is large compared to the computational grid, this can be resolved by the accretion code. This can be seen in the LEWICE/NS[8] example shown in Fig. 18. provided by Dr. Mark Potapczuk. A feather and the resulting interstitial gap can be seen to grow normal to the forward surface of the large roughness element. It should be noted that this is much larger than the feathers observed by video. However, nothing in the physics of the codes precludes reducing the computational scale to a point where small feather growth could be resolved.

In many cases computational resources would prohibit direct calculation of feather growth. However, freezing-fraction-enhancement models can be developed to determine how far into the boundary layer a roughness element must penetrate before the freezing fraction approaches unity.

Conclusions

In conclusion, high magnification observations of the off-stagnation regions where horns initiate in glaze-ice accretion have been observed on several simple cylindrical bodies in the NASA Lewis Icing Research Tunnel. These observations indicate that "feather" growth into the direction of flow is prevalent in the horn regions for *Rime*, *Mixed*, and some glaze horned accretions (*Type A* Horns). In very wet conditions, surface water runback dominates the off stagnation region and a different type of glaze horn growth is observed (*Type B* Horns). The feather observations are consistent with a dry-rime ballistic accretion model proposed by Personne.[4] The surface-normal characteristic of wet-ice growth and the into-flow growth characteristic of feather-ice growth may be modeled either by making the computational grid sufficiently fine or by including different growth models in the stagnation and feather regions.

Acknowledgments

The portion of this work performed at MIT was supported in part by NASA and FAA Grants NAG–3–666 and NGL–22–0069–640. The authors would like to acknowledge the efforts of the groups supporting this test in the NASA Lewis Research Center Icing Research Tunnel (IRT). The Test Installations Division (TID), Aeropropulsion Facilities and Experiments Division (AFED), and Technical Information Services Division (TISD) personnel provided excellent support above and beyond that normally required for IRT testing. Specifically, without the support of James Sims of TISD and Victor Canacci of AFED this test would not have been possible.

References

1. Olsen, W., and Walker, E., "Experimental Evidence for Modifying the Current Physical Model for Ice Accretion on Aircraft Surfaces," NASA TM–87184, 1986.

2. Hansman, R.J., "Analysis of Surface Roughness Generation in Aircraft Ice Accretion," AIAA Paper 92–0298, Jan. 1992.

3. Soeder, R.H., and Andracchio, C.R., "NASA Lewis Icing Research Tunnel User Manual," NASA TM–102319, 1990.

4. Personne, P., "Effet de la Rugosite sur la Croissance du Givre a Faible Vitesse: Resultats Experimentaux et Modelisation," ScD Thesis, l'Universite Blaise Pascal (Clermont-Ferrand II), June 1988.

5. Al-Khalil, K.M., Keith, T.G., and Dewitt, K.J., "Development of an Improved Model for Runback Water on Aircraft Surfaces," AIAA Paper 92–0042, Jan. 1992.

6. Ruff, G.A., and Berkowitz, B.M., "Users Manual for the NASA Lewis Ice Accretions Prediction Code (LEWICE)," NASA CR–185129, 1990.

7. Gent R.W., "TRAJICE2—A Combined Water Droplet Trajectory and Ice Accretion Prediction Program for Aerofoils," Royal Aerocraft Establishment, Farnborough, England, Report RAE TR–90054, 1990.

8. Potapczuk, M.P., and Al-Khalil, K.M., "Ice Accretion and Performance Degradation Calculations with LEWICE/NS," AIAA Paper 93–0173, Jan. 1993.

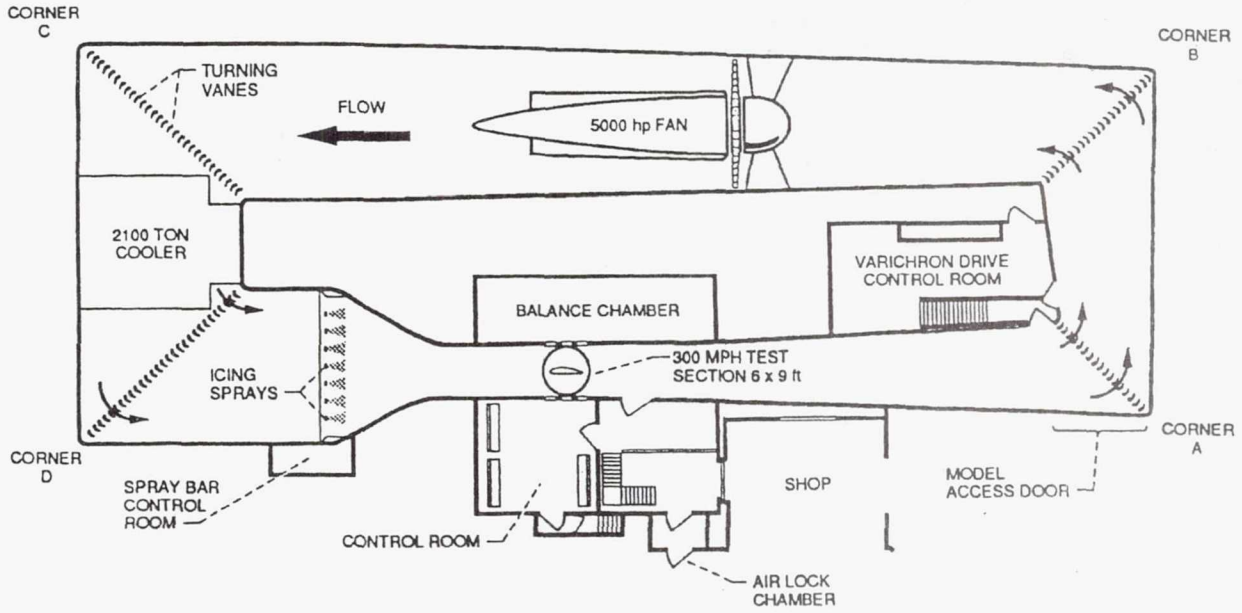

Figure 1.—Layout of the NASA Lewis Research Center Icing Research Tunnel.

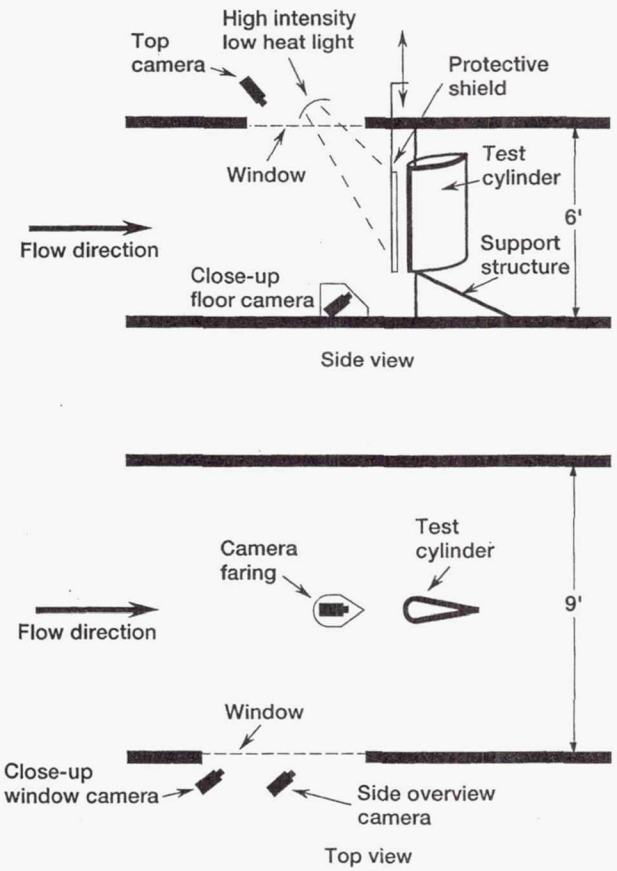

Figure 2.—Side and top views of the experimental set-up.

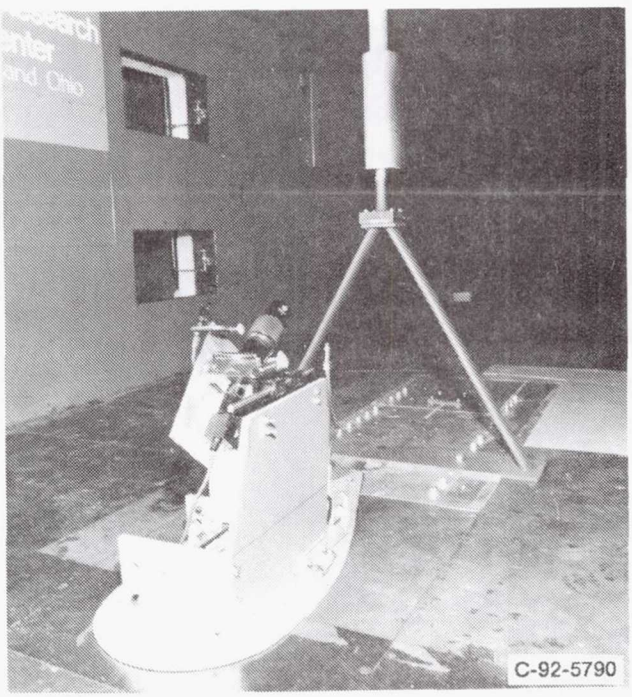

Figure 3.—Floor mounted camera assembly without fairing.

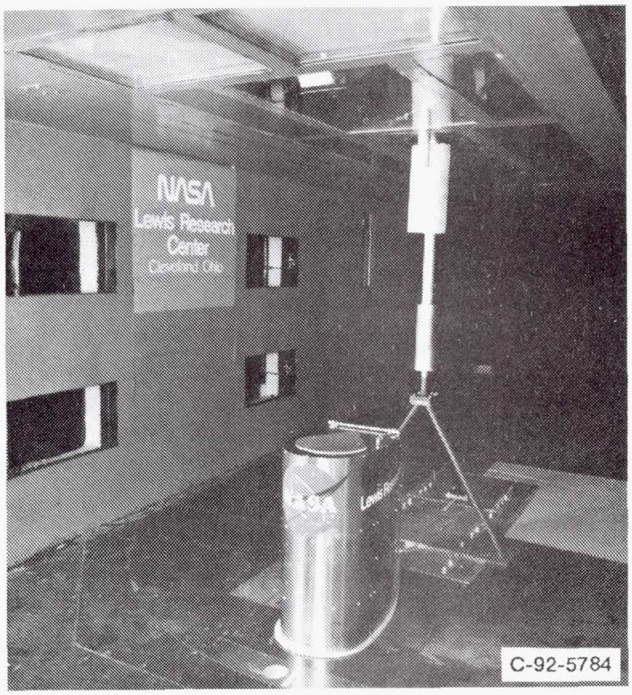

Figure 4.—Floor mounted camera assembly with fairing.

Figure 5.—Telescopic close-up camera assembly.

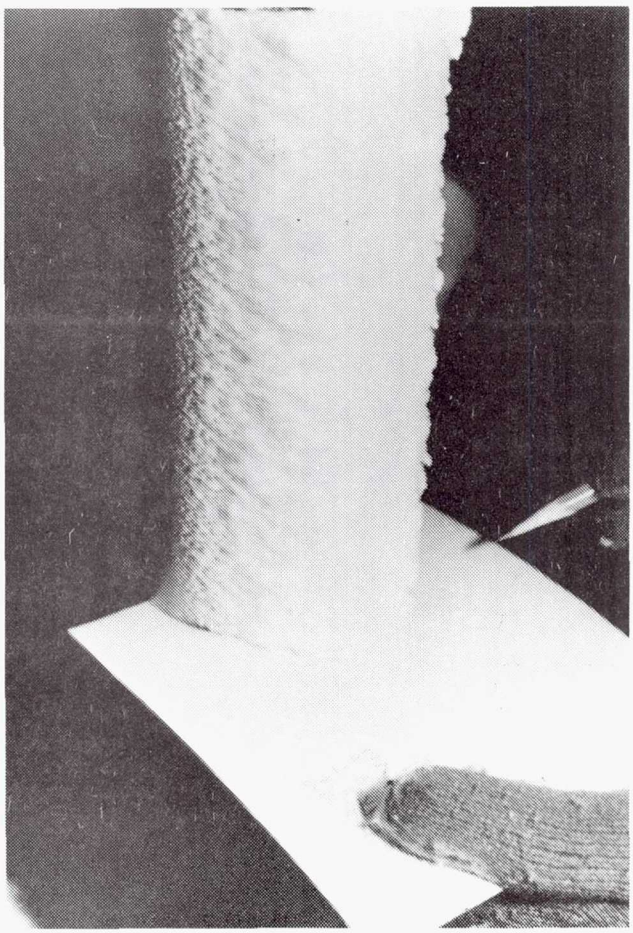

Figure 6.—Tracing of ice shape onto cardboard template.

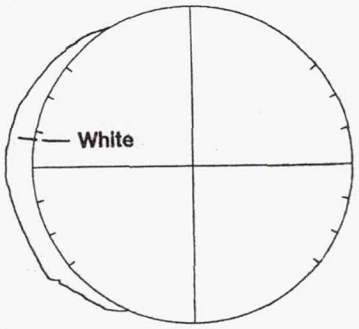

(a) RIME; 67 m/s (150 mph), 0.5 g/m^3, 20 μm, −26 °C (−15 °F) 7 min.

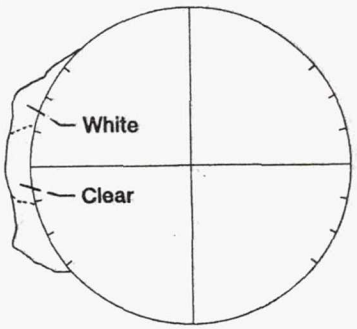

(b) Mixed; 89 m/s (200 mph), 0.32 g/m^3, 15 μm, −4 °C (25 °F) 12 min.

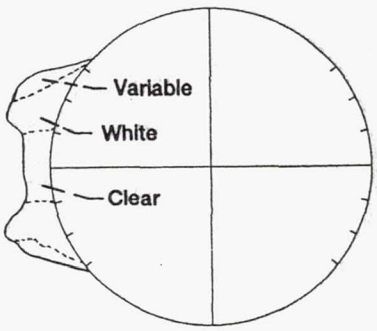

(c) Horn A; 89 m/s (200 mph), 0.5 g/m^3, 20 μm, −4 °CF (25 °F), 12 min.

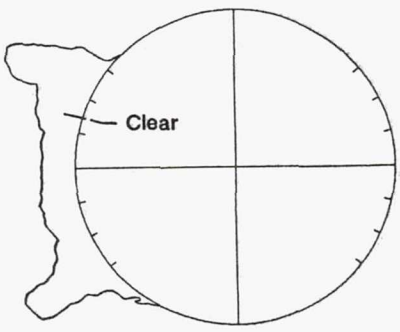

(d) Horn B; 67 m/s (150 mph), 1.0 g/m^3, 20 μm, −4 °C (25 °F), 12 min.

Figure 7.—Ice accretion types observed.

Figure 8.—Example of feather growth; 44 m/s (100 mph), 0.7 g/m^3, 15 μm, −15 °C (5 °F).

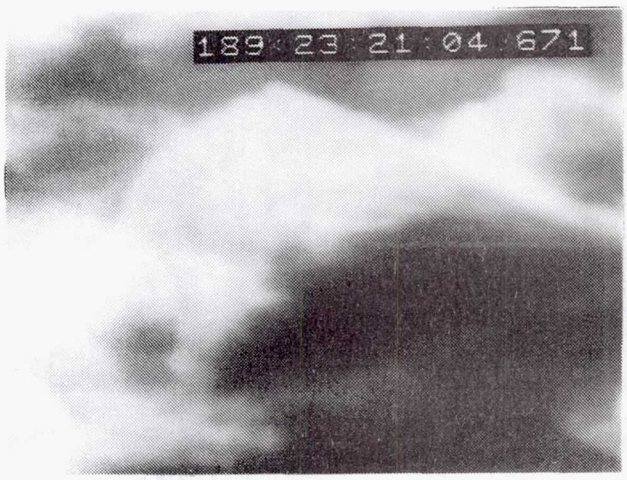

Figure 9.—Example of feather growth; 89 m/s (200 mph), 0.7 g/m^3, 15 μm, −16 °C (−15 °F).

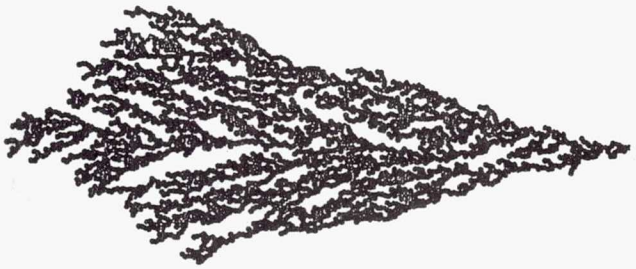

(a) Predicted feather shape (from Personne[4]).

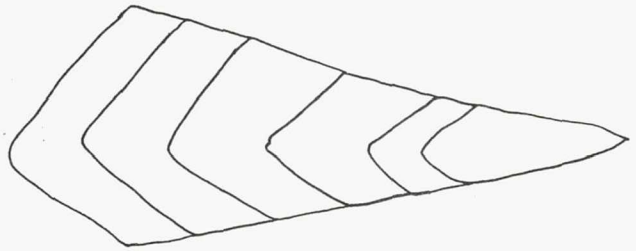

(b) Observed feather shape at 20 sec intervals; 44 m/s (100 mph), 0.7 g/m^3, 15 μm, –4 °C (25 °F).

Figure 10.—Predicted and observed individual feather shape.

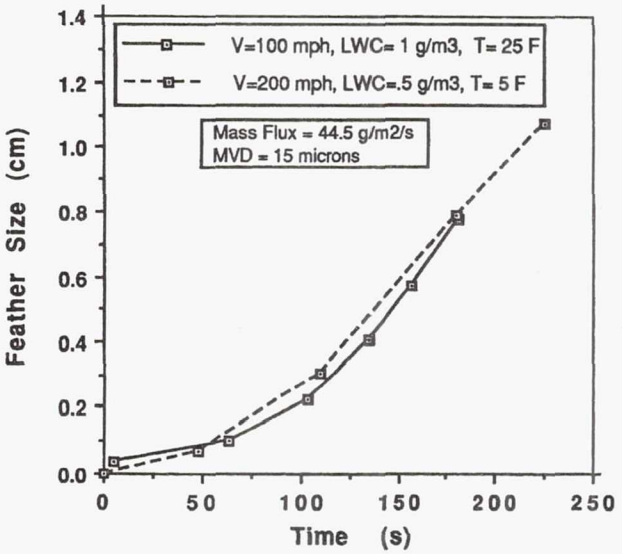

Figure 11.—Feather growth for two cases with constant mass flux.

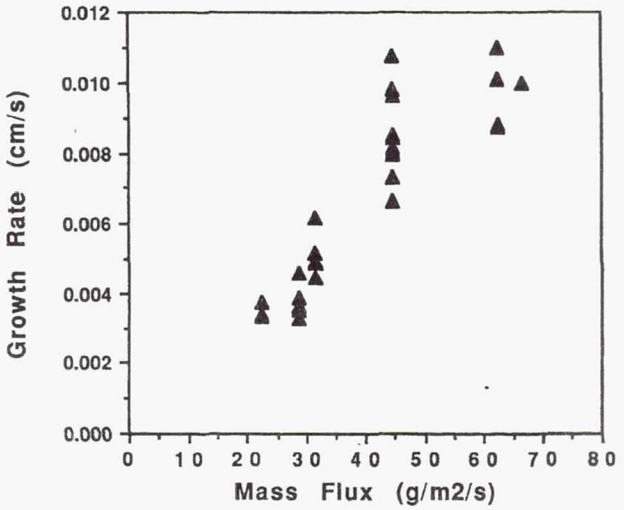

Figure 12.—Observed steady-state feather growth rates over a variety of operating conditions.

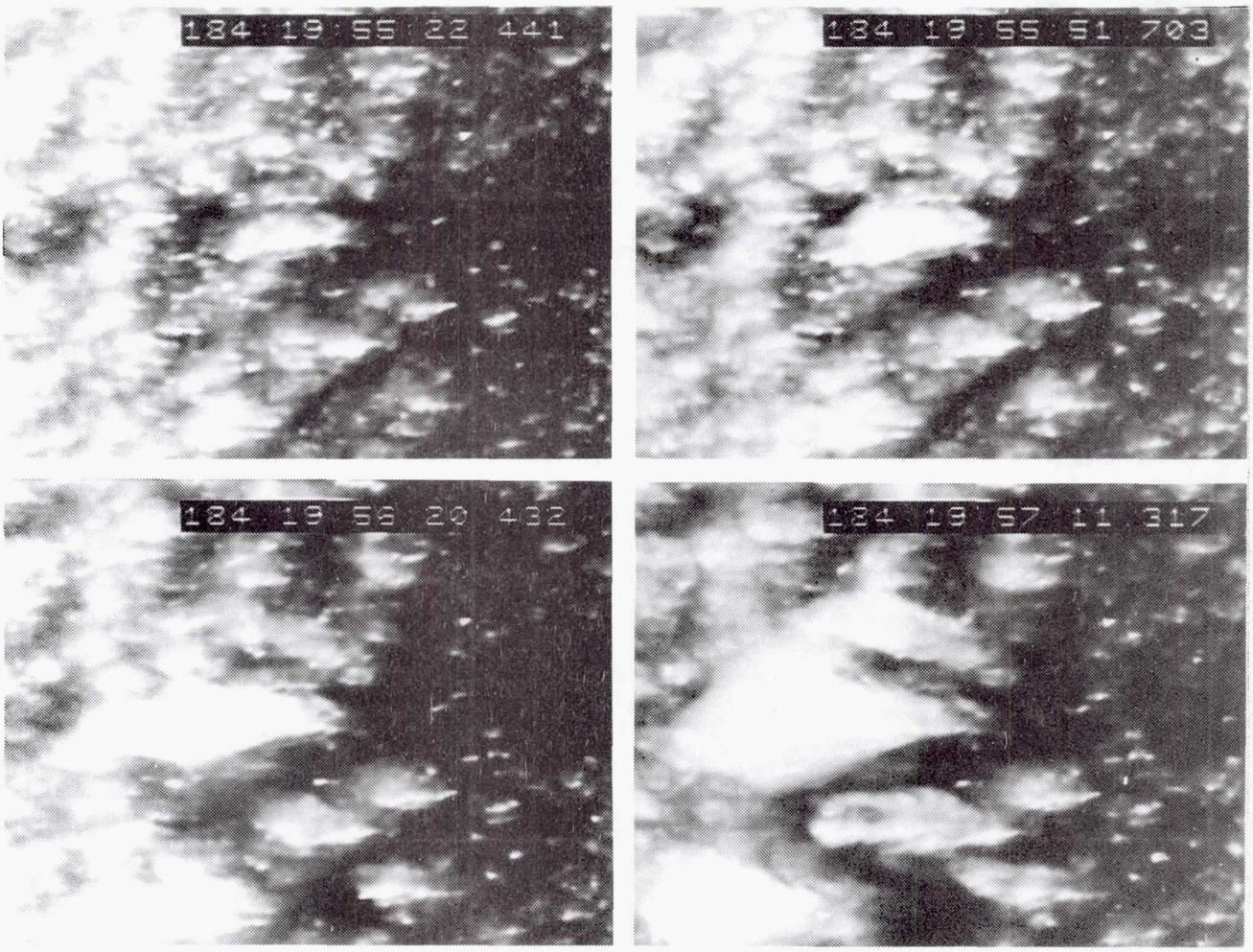

Figure 13.—Example of wet feather growth; 44 m/s (100 mph), 0.7 g/m^3, 15 μm, –4 °C (25 °F).

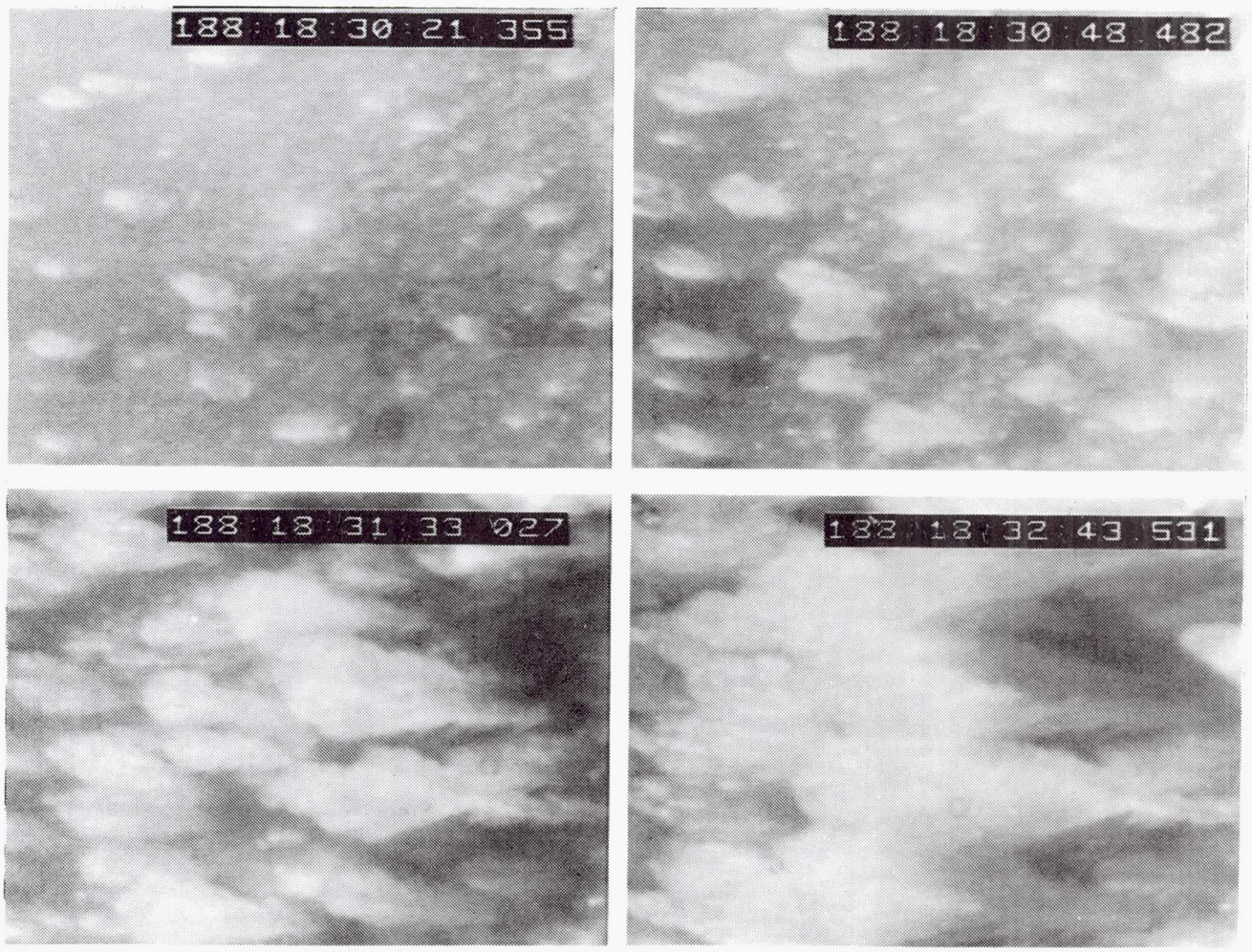

Figure 14.—Example of feather growth from nucleation site; 89 m/s (200 mph), 0.5 g/m^3, 15 μm, –4 °C (25 °F).

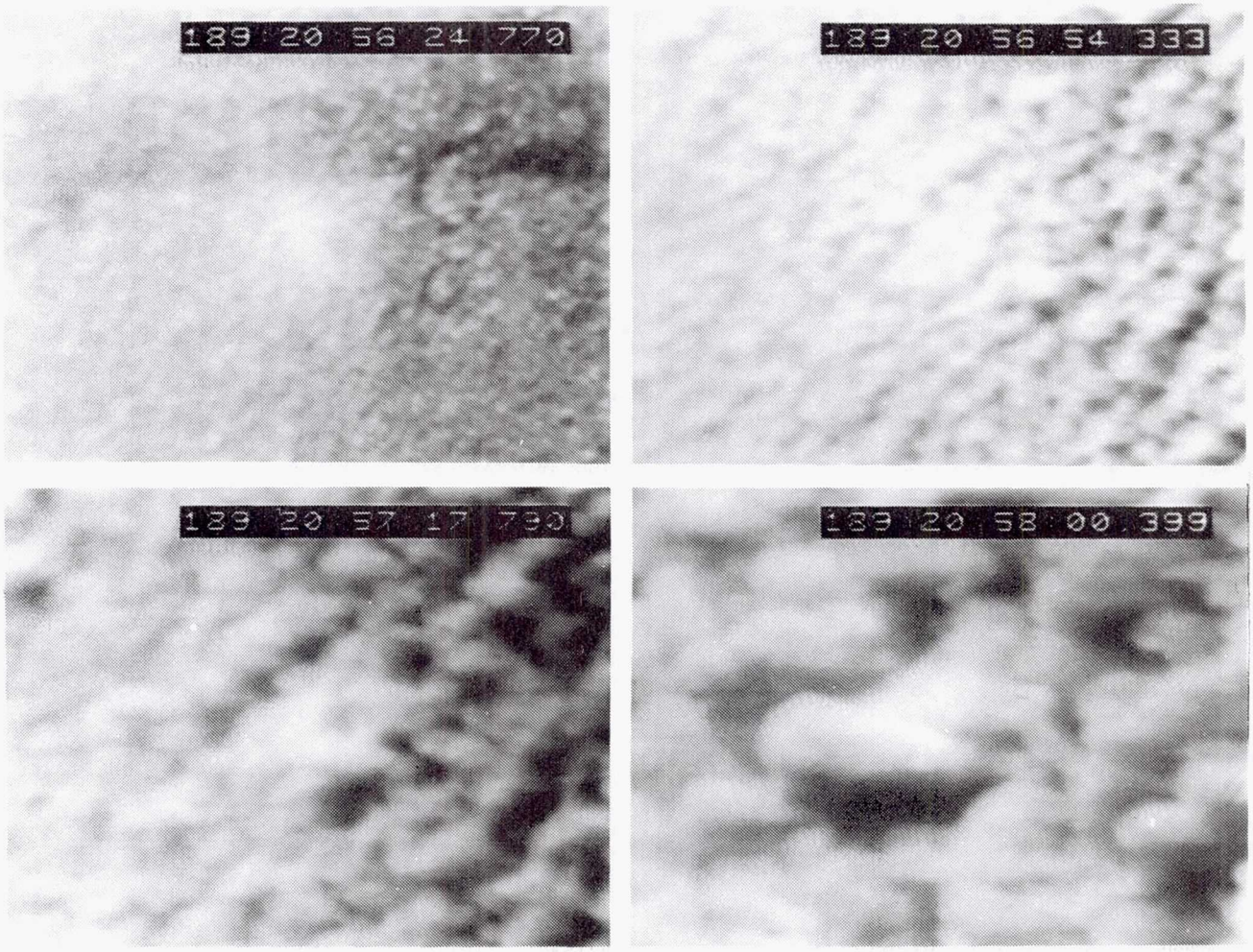

Figure 15.—Example of feather growth from clean surface; 89 m/s (200 mph), 0.7 g/m^3, 15 μm, –20 °C (–5 °F).

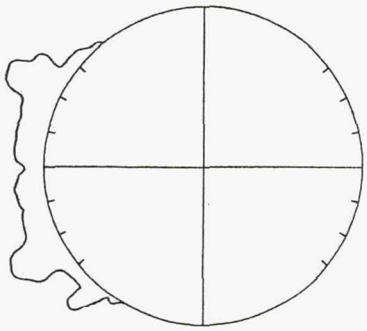

(a) 0.5 g/m^3.

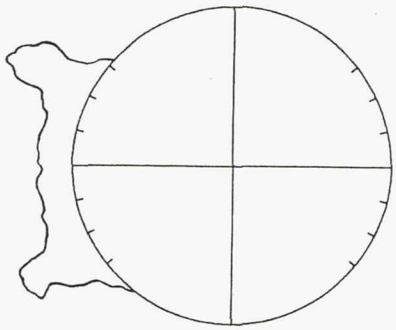

(b) 0.75 g/m^3.

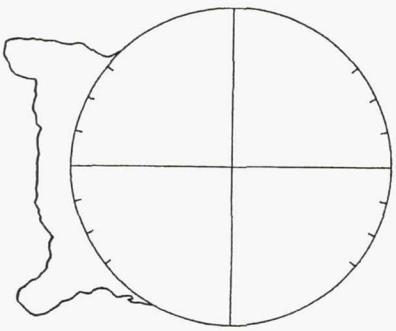

(c) 1.0 g/m^3.

Figure 16.—Effect of LWC on type B horns; 67 m/s (150 mph), 20 μm, –4 °C (25 °F).

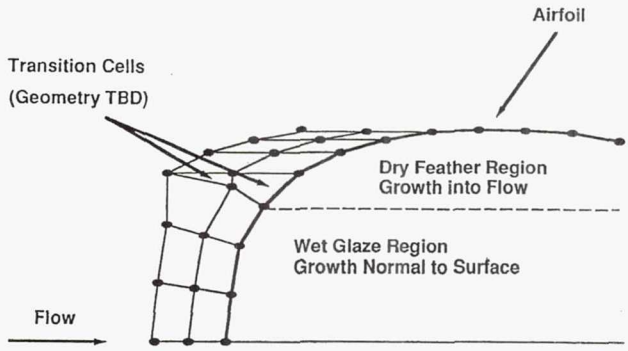

Figure 17.—Schematic example of how wet and dry growth could be implemented in LEWICE.

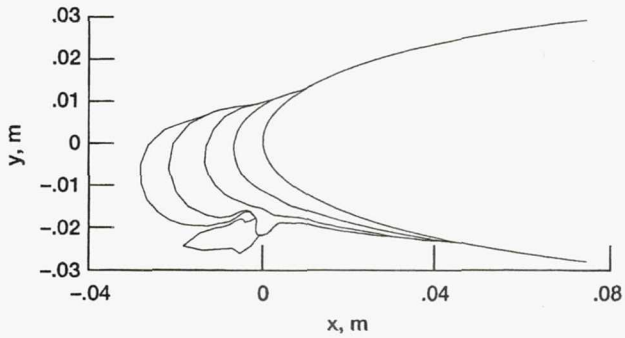

Figure 18.—Feather growth calculated with LEWICE/NS[9].

REPORT DOCUMENTATION PAGE

Form Approved
OMB No. 0704-0188

1. AGENCY USE ONLY (*Leave blank*)	2. REPORT DATE	3. REPORT TYPE AND DATES COVERED
	January 1993	Technical Memorandum

4. TITLE AND SUBTITLE

Close-up Analysis of Aircraft Ice Accretion

5. FUNDING NUMBERS

WU–505–68–10

6. AUTHOR(S)

R. John Hansman, Kenneth S. Breuer, Didier Hazan,
Andrew Reehorst and Mario Vargas

7. PERFORMING ORGANIZATION NAME(S) AND ADDRESS(ES)

National Aeronautics and Space Administration
Lewis Research Center
Cleveland, Ohio 44135–3191

8. PERFORMING ORGANIZATION REPORT NUMBER

E–7473

9. SPONSORING/MONITORING AGENCY NAMES(S) AND ADDRESS(ES)

National Aeronautics and Space Administration
Washington, D.C. 20546–0001

10. SPONSORING/MONITORING AGENCY REPORT NUMBER

NASA TM–105952
AIAA–93–0029

11. SUPPLEMENTARY NOTES

Prepared for the 31st Aerospace Sciences Meeting and Exhibit sponsored by the American Institute of Aeronautics and Astronautics, Reno, Nevada, January 11–14, 1993. R. John Hansman, Kenneth S. Breuer, and Didier Hazan, Department of Aeronautics and Astronautics, Massachusetts Institute of Technology, Cambridge, Massachusetts 02139 and Andrew Reehorst and Mario Vargas, NASA Lewis Research Center. Responsible person, Andrew Reehorst, (216) 433–3938.

12a. DISTRIBUTION/AVAILABILITY STATEMENT

Unclassified - Unlimited
Subject Category 03

12b. DISTRIBUTION CODE

13. ABSTRACT ***(Maximum 200 words)***

Various types of ice formation have been studied by analysis of high magnification video observations. All testing was conducted in the NASA Lewis Research Center's Icing Research Tunnel (IRT). A faired 8.9 cm (3.5 in.) diameter metal-clad cylinder and a 5.1 cm (2 in.) aluminum cylinder were observed by close-up and overview video cameras for several wind tunnel conditions. These included close-up grazing angle, close-up side view, as well as overhead and side overview cameras. Still photographs were taken at the end of each spray along with tracings of the subsequent ice shape. While in earlier tests only the stagnation region was observed, the entire area from the stagnation line to the horn region of glaze ice shapes was observed in this test. Two modes of horn formation have been identified within the range of conditions observed. In the horn region, Horn Type A ice is formed by "dry" feather growth into the flow direction and Horn Type B is formed by a "wet" growth normal to the surface. The feather growth occurs when the freezing fraction is near unity and roughness elements exist to provide an initial growth site.

14. SUBJECT TERMS

Aircraft icing; Surface roughness; Ice accretion; Heat transfer

15. NUMBER OF PAGES

14

16. PRICE CODE

A03

17. SECURITY CLASSIFICATION OF REPORT	18. SECURITY CLASSIFICATION OF THIS PAGE	19. SECURITY CLASSIFICATION OF ABSTRACT	20. LIMITATION OF ABSTRACT
Unclassified	Unclassified	Unclassified	